A New Integral Field Spectrograph for Exoplanetary Science at Palomar

Sasha Hinkley*[a,b], Ben R. Oppenheimer[b], Douglas Brenner[b], Ian R. Parry[c], Anand Sivaramakrishnan[b], Remi Soummer[b], David King[c]
[a]Department of Astronomy, Columbia University, 550 W. 120th St. , New York, NY, USA 10027;
[b]Department of Astrophysics, AMNH, 79th St. at Central Park West, New York, NY, USA 10024;
[c]Institute of Astronomy, Cambridge CB3 0HA United Kingdom

ABSTRACT

In July 2008, a new integral field spectrograph and a diffraction limited, apodized-pupil Lyot coronagraph was installed behind the adaptive optics system at the Hale 200-inch telescope at Palomar. This instrument serves as the basis of a long-term observational program in high-contrast imaging. The technical goal is to utilize the spectral nature of speckle noise to overcome it. The coronagraph alone will achieve an initial dynamic range of 10^{-5} at 1", with first light in mid-2008, without speckle noise suppression. Initial work indicates that spectral speckle suppression will provide a factor of 10 to 100 improvement over this. Such sensitivity provides detection and low resolution spectra of young planets of several Jupiter masses around young stars within 25 pc. The spectrograph obtains 32 images across the J and H bands (1.05 - 1.75 μm), with a spectral resolution of 30-100. The image plane is subdivided by a 200 x 200 element micro-lenslet array with a plate scale of 21 mas per lenslet, diffraction-limited at 1.0 μm. Data is collected with a 2048 x 2048 pixel Rockwell Hawaii-II HgCdTe infrared detector cooled with liquid Nitrogen. This system is the first of a new generation of apodized pupil coronagraphs combined with high-order adaptive optics and integral field spectrographs.

Keywords: High Contrast Imaging, Coronagraphy, Adaptive Optics, Exoplanets, Integral Field Spectroscopy
*shinkley@astro.columbia.edu; phone 1 212 313-7631; fax 1 212 769-5007; www.astro.columbia.edu/~shinkley

1. INTRODUCTION

1.1 Exoplanetary Science

In recent years, astronomers have identified nearly 300 planets outside our solar system, launching the new and thriving field of exoplanetary science. The diversity of the findings has been stunning. We have discovered stellar systems that host multiple massive planets, similar to the outer gas giant planets in our own solar system. Others possess "hot Jupiters" orbiting their stars in only a few days. To date, all of these objects have been discovered indirectly by observing the variations in their host star's light. Surveys employing the well-known Doppler effect due to the gravitational wobble induced on the host stars provide orbital eccentricity, semi-major axes, and upper limits on the masses of companion planets. Transit surveys provide exciting data on planet radii and limited spectroscopy of the planets themselves. However, to study the vast diversity of this population of objects, which may be more numerous than stars themselves, requires direct observation free of contamination from the primary stars, and with weaker observational biases over the parameter space planets occupy.

This is the core of a new field called comparative exoplanetary science. Direct imaging surveys hold the promise of quickly settling some of the most basic puzzles about exoplanetary systems, such as the fraction of stars hosting planets, or this fraction's dependence on stellar environment. We can also quickly survey planetary architectures, i.e. the distribution of planets at various orbital radii. The orbital placement of companions will enlighten ongoing work into planetary migration, and help to constrain models of planet formation and evolution. Once the instrumentation and techniques are fully in place, direct detection will be an extremely efficient method of discovery.

The ultimate goal of direct imaging surveys is not just to examine planet orbital parameters and the related implications for formation scenarios. Direct imaging enables spectroscopy, the doorway and key to unlocking the detailed properties

Adaptive Optics Systems, edited by Norbert Hubin, Claire E. Max, Peter L. Wizinowich,
Proc. of SPIE Vol. 7015, 701519, (2008)
0277-786X/08/$18 · doi: 10.1117/12.789557

of the objects themselves. Spectroscopy provides clues to the atmospheric chemistry, internal physics, geology, and perhaps even biological activity within or on these objects. More robust classification schemes for planets in general will arise from observing as many planets as possible at different ages, in different environments, and with a broad range of parent stars.

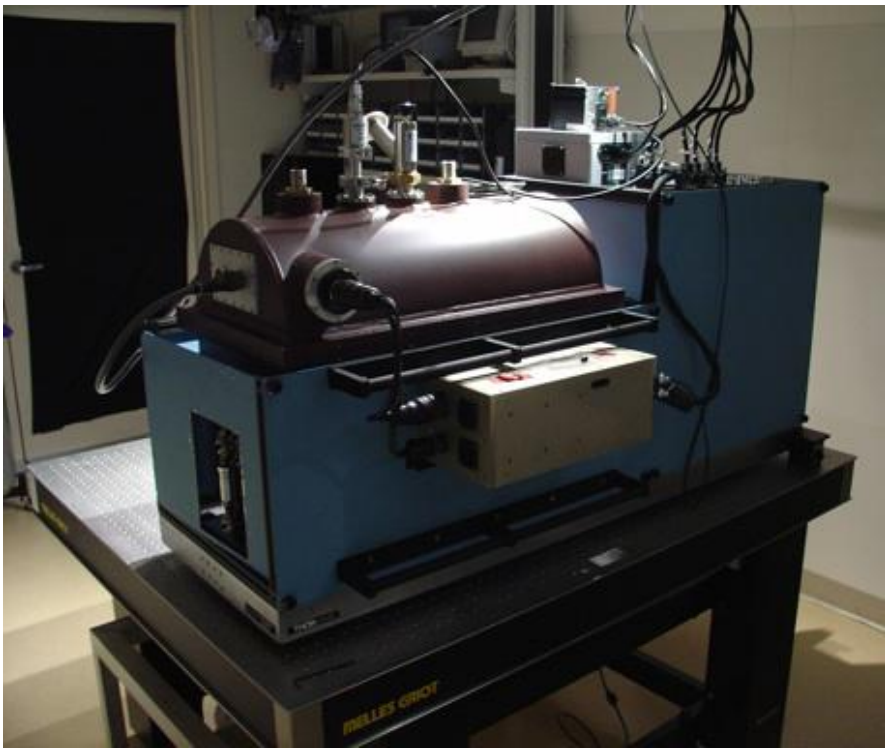

Fig. 1. The integral field spectrograph (purple dewar) integrated with our apodized-pupil coronagraph (behind blue enclosure panels). The instrument will be coupled to the Palomar Adaptive Optics (PALAO) bench inside the Cassegrain cage on the 200" Hale Telescope.

1.2 High Contrast Imaging

The major obstacle to the direct detection of planetary companions of nearby stars is the overwhelming brightness of the host star. If our solar system were viewed from a nearby star, Jupiter would appear 10^7-10^8 times fainter than our Sun in the near-IR and would be completely lost in its glare. Very large telescope apertures, although extremely efficient for building up signal, are not a necessity for direct imaging of companions. The key requirement is the suppression of the star's overwhelming brightness (Oppenheimer et al. 2003, Hinkley et al. 2007).

A promising method for direct imaging of stellar companions involves two techniques working in conjunction. The first, high-order Adaptive Optics (AO), provides control and manipulation of the image by correcting the aberrations in the starlight's wave front caused by the Earth's atmosphere. Second, a Lyot coronagraph (Lyot 1939, Sivaramakrishnan et al. 2001) suppresses this corrected light. Together, these two techniques can obtain contrast levels of 10^5 or better. Our team has been using these techniques for several years at the AEOS telesope in Maui under the name "The Lyot Project." (Oppenheimer 2003, 2004, and Sivaramakrishnan 2007). Direct imaging projects such as the Lyot Project are pushing the detection boundaries into the region of parameter space only previously probed by Doppler surveys. Improvements in coronagraphy, specifically the apodization of the telescope pupil (Soummer 2003, 2005), can increase the contrast by factors of 10 to 100 as well. Our new project, dubbed "Project 1640" incorporates all of these advances with an integral field spectrograph to aid in removal of background noise due to speckles.

1.3 Speckle Noise

The combination of techniques described above, coronagraphy and high-order adaptive optics, is perhaps the most promising method of direct imaging. But this combination of techniques, like any form of high contrast imaging, still suffers from a significant source of noise, limiting the detection sensitivity. Small aberrations in the incoming stellar

wave front, arising from imperfections in the AO optics or the coronagraphic optics, can lead to a pattern of speckles that litter the image in the focal plane. These speckles are the single largest hindrance to the detection of faint companions around nearby stars. Without a coronagraph, Racine et al. (1999) has demonstrated that speckle noise will dominate over photon noise by a factor of $\sim 10^2$ to 10^3. Such speckle noise is largely due to non-common path errors (those not measured by the wave front sensor), e.g., small aberrations in the coronagraphic optics, as small as 1 nm. Other sources include AO correction errors such as fitting error, aliasing, lag, and Fresnel wave front propagation effects. Speckle noise is also highly correlated and thus not surmountable with simple techniques such as long exposures, or using larger and larger telescopes (Hinkley et al. 2007, Soummer et al. 2007).

The suppression of speckle noise is paramount in the direct detection problem. Within the Lyot Project we have already explored two such methods of speckle suppression. One method involves simply subtracting speckles that are highly stable in time with software. This method has improved our detection sensitivity by about one to two magnitudes (Hinkley et al. 2007, Leconte et al. 2007, Marois et al 2006), a factor of a few to ten. Another method uses a dual-imaging polarimetry (Kuhn et al. 2001, Perrin et al. 2004, Oppenheimer et al. 2008, Hinkley 2008 forthcoming). This technique is extremely powerful, essentially eliminating the speckle noise from the unpolarized speckle pattern and greatly increasing our sensitivity to polarized objects, such as circumstellar disks, achieving 10^{-5} contrast at 0.3" separation (Oppenheimer et al. 2008). However it is limited to the study of polarized sources.

Another speckle suppression technique promises to eliminate speckle noise but without the limitation that the target of observation exhibit polarization, thereby opening up the regions of close proximity to nearby stars to full astrophysical study. The speckle noise pattern is an optical phenomenon, and its shape and morphology change with wavelength. Indeed, the position of each speckle will change with wavelength. A true astronomical object, of course, will remain stationary as a function of wavelength. This method, sometimes referred to as "spectral deconvolution" has been described before (e.g. Sparks and Ford 2002). To take advantage of the spectral nature of the speckle noise, we have built an integral field spectrograph, coupled to an Apodized-pupil Lyot Coronagraph. This is the first integral field spectrograph to be placed behind a coronagraph and coupled to a high-order AO system.

2. INTEGRAL FIELD SPECTROGRAPH DESIGN

We have built a lenslet-based integral field spectrograph covering 1.05 – 1.75 μm with a 4 arcsecond field of view. This will allow us to obtain course spectra (R ~ 30) at every point in the image. The coronagraph is descirbed in §3.

2.1 Optical Design

The optical design for our integral field spectrograph is shown in Figure 3 below. The overall design can be categorized into four components: a lenslet array; a dioptric collimator with a 200 mm focal length consisting of five lenses made up of three different glasses (SK8, SF2, BaF_2) which reimages the telescope pupil on the prism; a prism/disperser element; and a camera component. All our transmissive optics, except for the lenslet array were manufactured by Janos Technology, while the reflective optics were manufactured by Axsys technologies. We discuss each of these components in more detail below.

The optical design has been fully modeled using the Zemax design software, including the effects of thermal contraction as the system is cooled. The system does not perform at room temperature. All optics with the exception of the lenslet array are oriented square with the mounting platform (work plate). The orientation of the lenslet array is 18.43º from the normal vector to the work plate. The prism is oriented to disperse the light parallel to the workplate. This places the detector square with the mounting plate as well, requiring only a rotation on the lenslet array. Wavelength filtering is achieved with J and H-band filter (1.05 – 1.75 μm), with OD3-OD4 blocking outside this range, placed directly in front of the detector.

Lenslet Array: The square lenslet array, manufactured by MEMS Optical (Boston), consists of two powered faces etched into a 1mm thick wafer of fused silica. The first face, placed in the focal plane at the output of our coronagraph, has lenslets with a radius of curvature of 950 μm and is primarily used to separate the light from each segment of the image, so that the higher powered exit surface retains as much of the light as possible (with minimal loss due to roll-over between the lenslets). The rear face lenslets have a 159 μm radius of curvature to create the pupil images 280 μm behind the lenslet array substrate. The effective f-number of each lenslet is f/4, measured using the diagonal of each square

lenslet (106.1 μm). Each lenslet has a pitch of 75 μm. We have 270 x 270 lenslets on our array, but only use 200 x 200 lenslets. The array is mounted 4mm directly in front of the first lens of the collimator. The platescale for the spectrograph is 21 mas/lenslet.

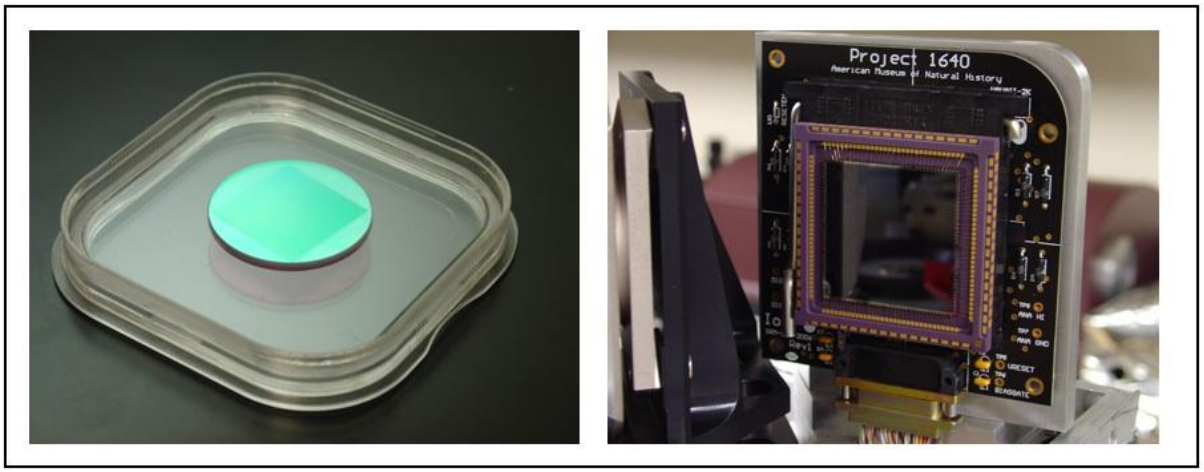

Fig. 2. Our lenslet array (left) and 2048 x 2048 Rockwell Hawaii-II HgCdTe infrared detector on its custom printed circuit board (right). Our 270 x 270 lenslet array has been etched onto a 30mm disk of fused silica, and each lenslet has a 75 μm pitch and f/4 focal ratio.

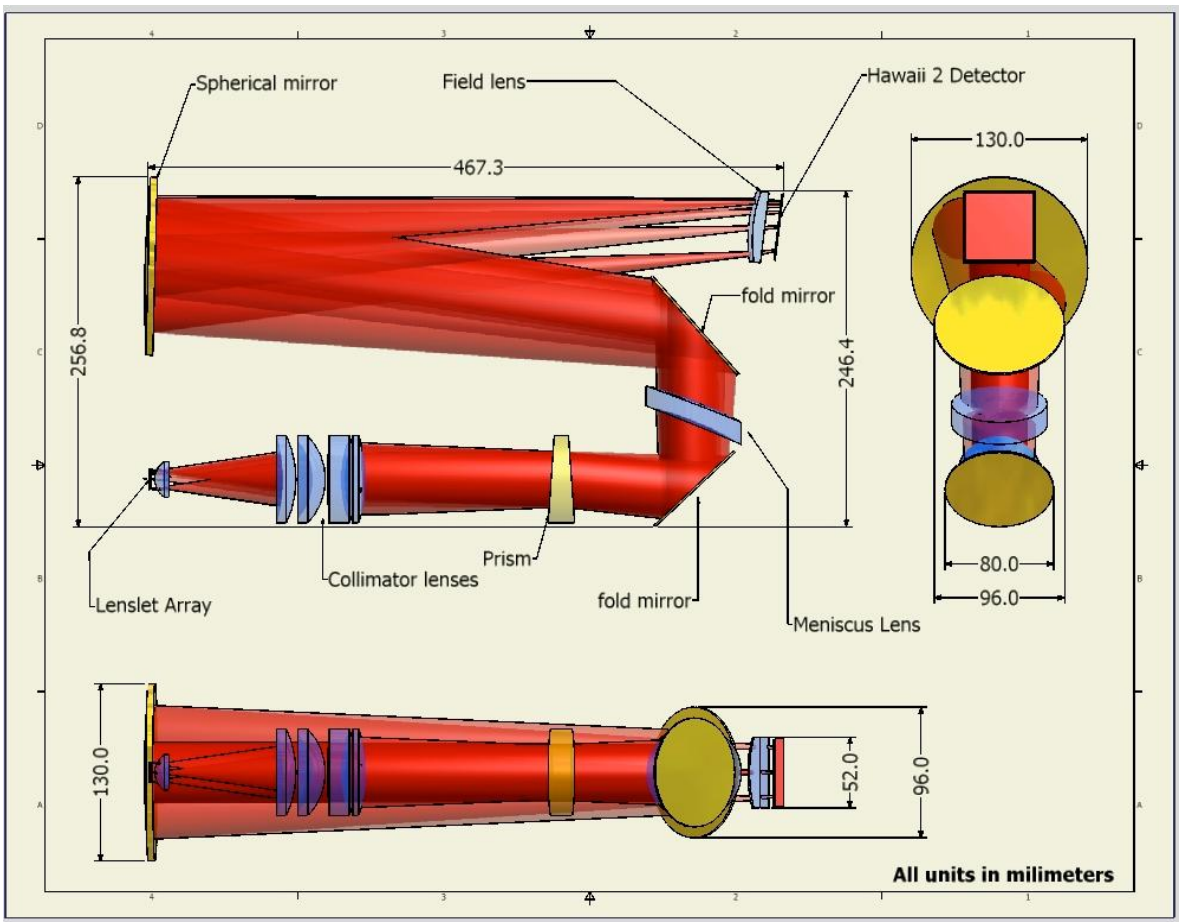

Fig. 3. Optical layout of our integral field spectrograph. A top view and two side views are shown for clarity.

Collimator: The collimator assembly consists of five lenses mounted in a single housing. The lens materials are: BaF2, SF2, and SK8. The collimator forms 40 mm pupil images at the prism's incident surface.

Prisms: Our prism is a single piece of BK7 glass, with a wedge angle of 4º on each face, 60mm in diamter and a central thickness of 15.135mm. This prism is optimized for the wavelength range (1.05 – 1.75 μm) with a dispersion direction parallel with the plane of the workplate.

Camera Optics: This consists of a meniscus corrector lens, spherical mirror, and a field-flattening lens ("field lens") in front of the detector. Both lenses are fused silica. The meniscus corrector lens has two surfaces with radii of curvature 216.82 and 227.90 mm, and was cored out of a larger (240mm diameter) parent lens. It is 14.4 mm thick, 70 mm in diameter and 80 mm off axis. The field lens creates a flat focal plane for the final detector. This lens is incorporated into the mount holding the detector and has adjustment capabilities in three-dimensions. This lens serves the double purpose of additional protection for the detector. The field lens has a rear flat surface and a front surface with radius of curvature of 105.55 mm. This lens is 57 mm square and 12mm thick. The sphere has a radius of curvature of 888.226 mm and a diameter of 130 mm. We also utilize two fold mirrors to accommodate packaging. All mirrors are made of diamond turned aluminum, coated with nickel, polished to λ/20 RMS surface error.

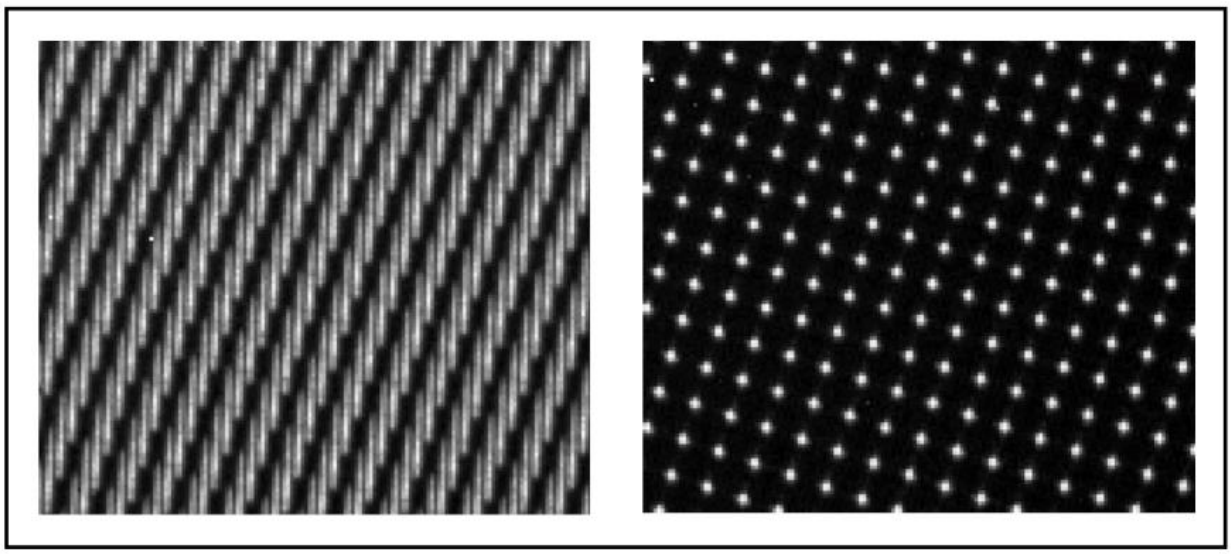

Fig. 4. Calibration images, showing a small section of the full array. These are raw data in which the lenslet array was uniformly illuminated. The left shows broadband spectra, while the right shows the expected spot pattern from a monochromatic laser at λ = 1330 nm.

2.2 Detector system

The heart of the detector system is a Rockwell Hawaii-II 2048x2048 pixel HgCdTe infrared array operating at cryogenic temperatures. The detector control uses a Generation III infrared array controller designed and built by Astronomical Research Cameras, Inc. (ARC) and configured to our Hawaii 2 chip. We also have a dedicated ARC power supply to go with this.

2.2.1 Detector system software

In order to maintain the greatest amount of flexibility and portability, our collaborators at the Astronomical Technology Centre in Edinburgh have configured our detector system to communicate with the outside world using XML files that are transferred using http (Beard et al 2002). The http protocol was chosen to allow greater flexibility and stability when such a system is moved from a particular institution or telescope. The XML files include all of the necessary parameters for a particular observation (exposure time, number of reads, etc). The system can perform Non-destructive reads (NDR)

as well as Correlated Double Sampling (CDS). The flow of the user commands is shown schematically in the figure below. The user sends the appropriate configuration XML files via http to a set of three separate, but connected servers setup on our Data Acquisition Computer that organize the camera operations, the filesaving, and the detector de-multiplexing. The user can directly communicate with the Camera and Filesave servers, but the Filesave server is the only module that will communicate with the de-multiplexing server.

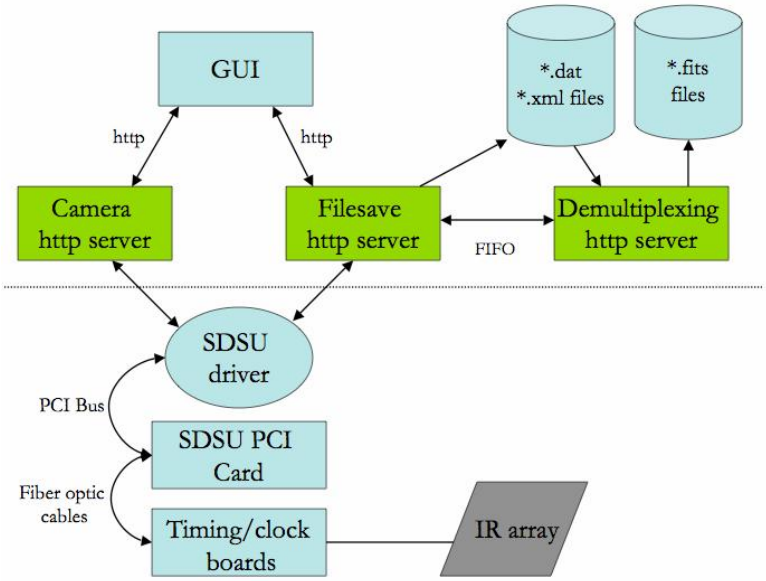

Fig. 5. A schematic diagram of our detector system operations. Three http servers (green boxes) handle communications between the user and the detector hardware via XML files. More detail on our system can be found in Beard et al., (2002).

We communicate directly to our Camera and Filesave servers using customized LabVIEW software. These servers communicate with the SDSU detector controller, which in turn, organizes the reading of the infrared array through the timing and clock boards. When an exposure is complete, the data files are stored in a raw data format, and the de-multiplexing http server converts these into FITS files.

2.3 Mechanical Design

We are required to operate our infrared array at cryogenic temperatures, and hence a cryogenic vacuum chamber dewar is required. This sections describes the features of many of the mechanical aspects of this project.

2.3.1 Dewar

Our cryogenic dewar is very similar to that used for the PHARO infrared camera at Palomar (Hayward et al. 2001). Our dewar was built in 2006 by Precision Cryogenics in Indianapolis, Indiana. The dewar is made almost entirely of 6061-T6 Aluminum with an outer shell divided into an upper and lower part. The upper half ranges from ¼ to ¾ inches in thickness and provides strong support for the overall assembly, while the lower part is lighter weight. These two halves wrap around the workplate, the inner heat shields, and the two Liquid Nitrogen (LN2) tanks and each half has a ¾ inch flange, or lip, where the two are joined. The optics workplate is comprised of a 1-inch thick, light-weight piece of Aluminum and is mounted to the outside of the dewar, at the lower flange, by four G-10 fiberglass mounting tabs. These tabs help the workplate to be thermally insulated from the outside of the dewar. The assembly will have a mounting bracket (see Figure 6 below) to provide focus movement and prevent any flexure while the telescope is rotated. While at Palomar, the whole assembly will hang down from the AO bench.

The bottom half of the Project 1640 dewar is the same as that for PHARO, but mirrored internally so that the detector is on the opposite end of the dewar from the window. We maintain our temperature near 77K, with 0.01 K rms stability. The LN2 fill holes are in the same place as on PHARO, but unlike PHARO's five ports, this dewar has four ports: two for the LN2 inputs into each can, one for the vacuum pump, and another for attachment of a vacuum guage.

Radiation shielding and Liquid Nitrogen tanks: Inside the outer surface of the dewar are the upper and lower radiation shields. The shields are wrapped in multiple layers of mylar insulation. Like the PHARO dewar, the Project 1640 dewar has two separate LN2 tanks: a 3.3L inner can directly bolted to the optics base plate, and a larger 11L can maintaining close contact with the radiation shield. This larger tank serves as the more global dewar cooler, while the small can provides a local heat sink for the detector and optics. The large can is bolted to the workplate via three posts just behind the G-10 tabs. The dewar's internal parts remain at 77K for 60 hours without refilling the nitrogen tanks.

2.3.2 Mounting and flexure control

To maintain dewar stability while minimizing flexure during telescope slewing, have have developed a custom dewar handling bracket (Figure 6) and manufactured by Opticology in New York City. Our dewar has three mounting pins, two towards the front, and one on the rear face, which are used to attach to our mounting bracket. The entire bracket assembly is mounted on flexure-resistant rails which allows 20-30mm of focus movement using a fine-thread scew. This mounting bracket also allows a +/-10 degree tilt using a screw-jack mechanism at the rear of the dewar, allowing the entire dewar to pivot on its front two mounting pins by applying a vertical movement at the rear pin.

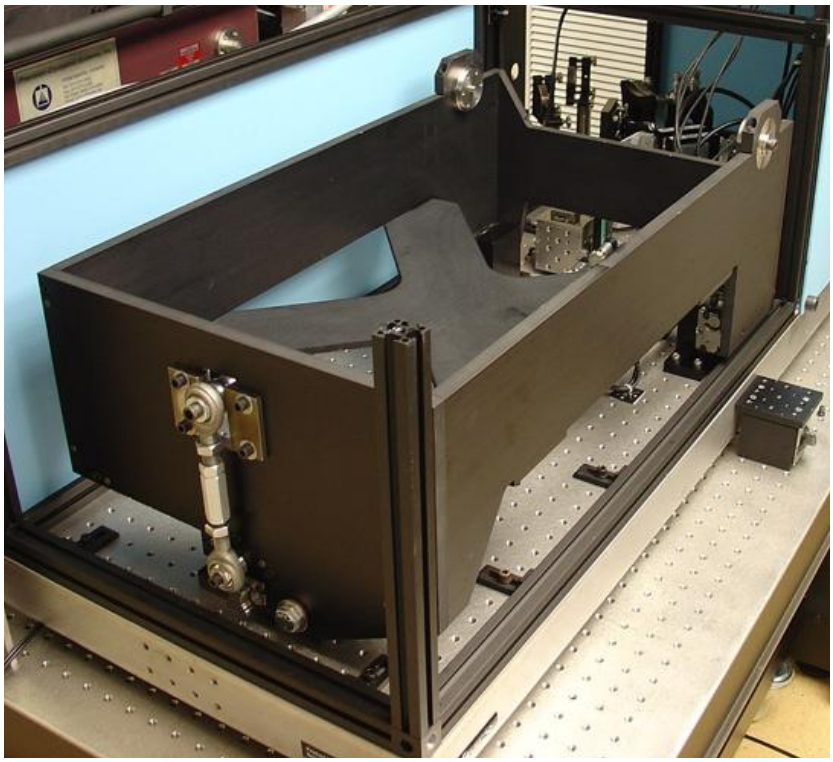

Fig. 6. The dewar handling and focus mechanism. This anodized aluminum rigid frame will help to prevent flexure, allow focus movement, and allows several degrees of tilt to be applied via the rear vertical jack mechanism shown above. The dewar is mounted in this frame via three points: the rear vertical jack screw, and two front pivot points. The entire assembly rides on flexure-resistant rails.

3. AN APODIZED-PUPIL LYOT CORONAGRAPH

To suppress the starlight of our target stars, we have built an apodized-pupil Lyot coronagraph based on the designs of (Soummer 2004, Sivaramakrishnan 2001). We achieve the majority of our suppression with a reflective focal plane mask (FPM) with a 1322μm diameter hole. We use the hole as an opaque mask and let the unocculted portion of the image around the hole be reflected on to the rest of the optical train. The light that has passed through the hole is used to drive our set of four infrared Hamamatsu tip/tilt sensors. The center of the stellar image is maintained on the sensors using a centroiding algorithm in conjunction with a control loop working with our fast-steering mirror (FSM). Our fast steering mirror is updated at a ~1 kHz frequency to maintain the position of the star on the center of the spot.

3.1 Coronagraphic layout

The layout of the coronagraph is shown in the figure below and is based on the concept of Sivaramakrishnan et al. (2001). The f/15.4 beam from the Palomar AO system enters our coronagraph via an infrasil window which counteracts some dispersion caused by the PALAO dichroic. The beam comes to a focus, strikes an OAP and is formed into a collimated beam. Next in the optical train is the apodizer. The beam then strikes the fast-steering mirror and continues onto the pair of atmospheric dispersion prisms (more detail on these is given below). The beam is brought back into a focus by an OAP in order to apply the primary coronagraphic correction at the Focal plane mask. The hole in the reflective mask serves as the occultor and the light travelling through the hole meets our infrared tip/tilt sensors. The unocculted portion of the image is reflected off the focal plane mask, and travels to another OAP which brings the beam back out of focus where it meets the Lyot stop. Similar to the focal plane mask, the Lyot stop is reflective, passing the unocculted portion of the image on to the rest of the system. Finally, this is brought to an image on our lenslet array of the spectrograph using a 600mm Spherical mirror (not shown in the figure below). The entrance beam into the spectrograph is a f/143 beam.

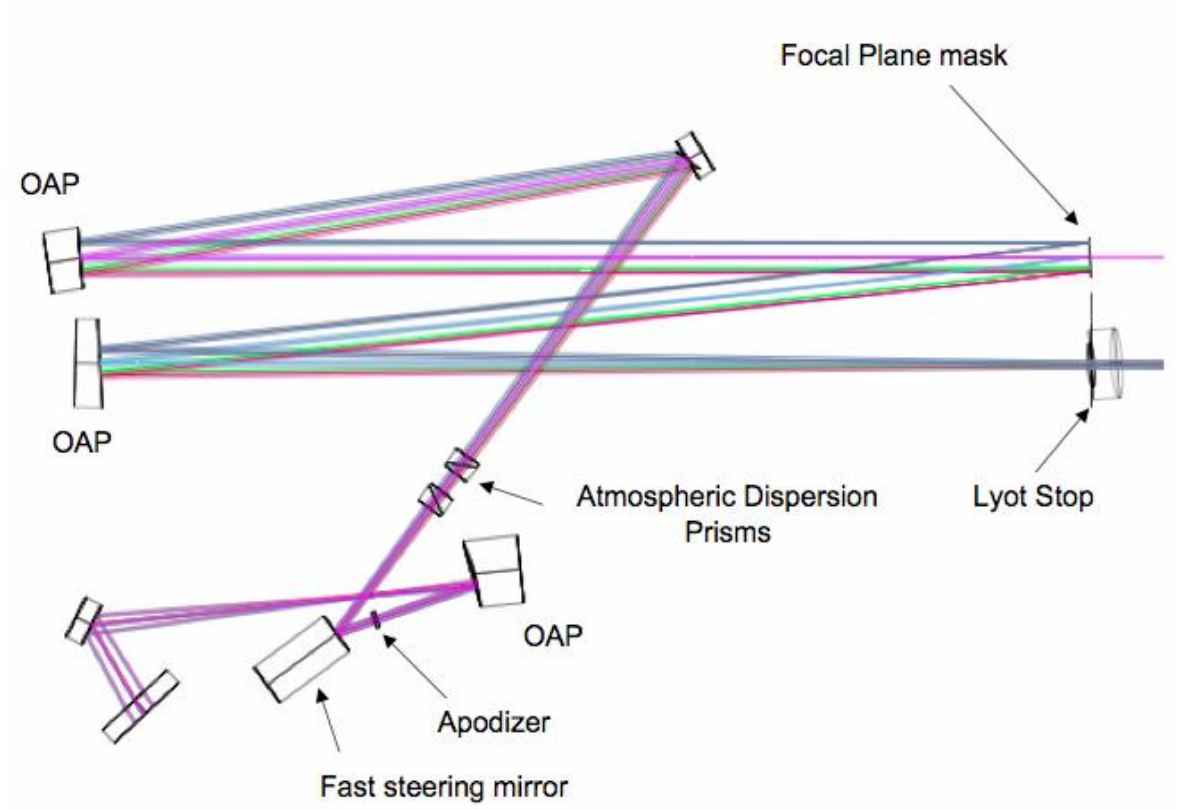

Fig. 7. The layout of our Apodized pupil Lyot Coronagraph (see text) taken from zemax. The design is based on the coronagraphy and apodization prescription described in Sivaramakrishnan et al. (2001) and Soummer et al. (2003), respectively. The system also has two sets of rotating prisms to correct for differential atmospheric refraction ("atmospheric dispersion"). Details of the various masks are given in the text and shown in Figure 8.

3.2 Masks

Our three masks are shown in Figure 8. Our apodizing mask is a 12.7mm transparent optic made by Jenoptik. It has a 3.9mm pupil and is shown in the photo below. The transmission profile on this mask follows the prolate spheroid apodization prescription as described in Soummer et al. (2003). The transmission profile is defined by a microdot pattern lithographically placed onto the suprasil substrate. The dots are placed on a 2 μm grid initially via electron-beam lithography, followed by a deposition of black chrome.

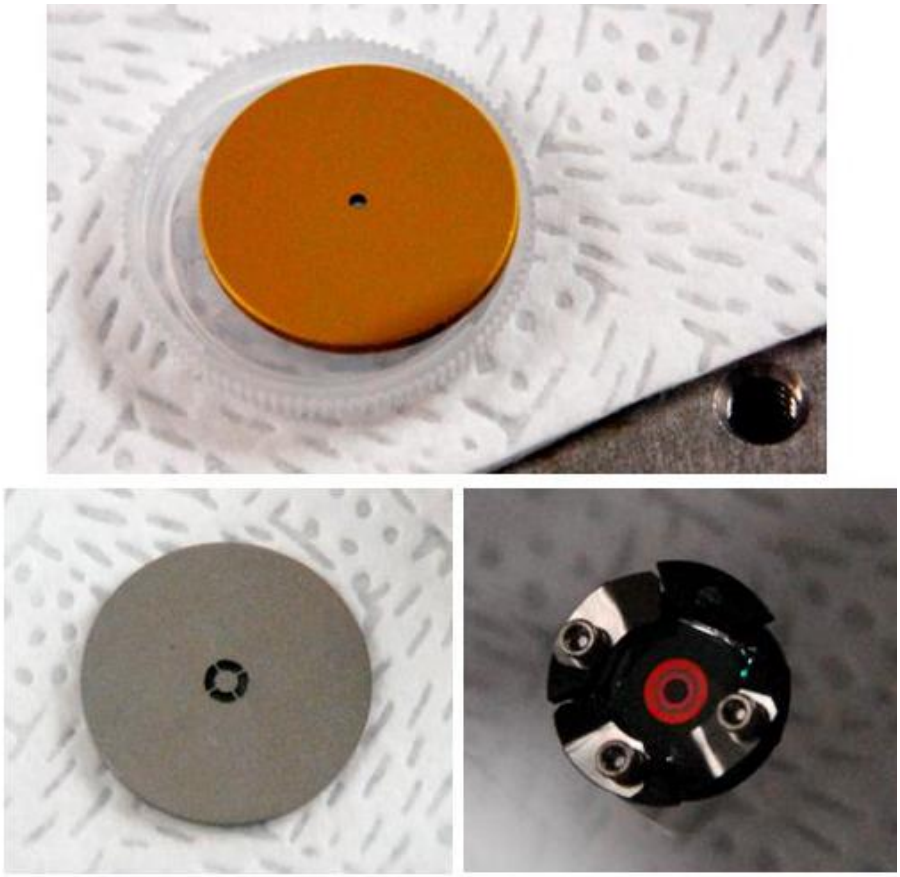

Fig. 8. Coronagraphic masks: Focal plane mask (top), Lyot mask (bottom left), and apodizer (lower right).

3.3 Infrared tip/tilt sensors

We are using an infrared position sensor comprised of four individual PIN photodiode detectors built by Hamamatsu (F6849 series). The detector area is 4 mm^2 and sensitive from 0.9 to 1.7 μm. Following correcting for flat field errors and dark subtraction, a simple centroiding algorithm is used to determine the stellar position. We estimate we can track stars of at least 7^{th} magnitude with a S/N of 4 under median conditions.

3.4 Correction for Differential Atmospheric Refraction

Refraction in the earth's atmosphere will cause the position of a star at one wavelength to differ from the position at another wavelength. From the blue edge of the J-band (~1.05 μm) to the red edge of the H-band (~1.75 μm), this displacement can be 100mas. To correct for this, we use two sets of Risley prisms via the prescription in Wynne (1996). Each prism set is constructed by coring out a cylinder from two cemented wedges of BaF_2 and CaF_2. The amplitude of correction is determined by the zenith angle of the target star and the positions of these prisms are update every second.

4. PALOMAR AO SYSTEM

4.1 Palomar AO system

The Palomar AO system (PALAO) is a 241-actuator AO system built by JPL for use on the 200-in Hale Telescope at Palomar (Dekany 1998). PALAO is currently being upgraded to a 3000-actuator system with a 64x64 Shack-Hartmann wave front sensor, and a new infrared tip/tilt sensor.

4.2 Integration with Palomar Adaptive Optics System

Our entire coronagraph+IFU package is mounted on a single Thorlabs custom breadboard 18" x 54" x 2.4" in size. One side of our breadboard has ¼-20 tapped holes on a one inch grid, suitable for mounting the coronagraphic optics and the

dewar mounting bracket. The other side of this breadboard contains four custom aluminum pucks for mounting the entire assembly to the Palomar AO system. The AO bench has an identical set of pucks attached in the same configuration. When the instrument is raised up to the bench, the four opposing sets of pucks are aligned and clamped together, with the dewar and coronagraphic optics hanging down. This procedure allows complete repeatability in each mounting.

We have also developed a customized handling cart for smooth instrument transport. The cart design aids in the installation on the AO bench primarily via two features: 1) Six spring housings cushion the transport as well as provide differential compression (As the instrument is raised up on the Cassegrain elevator, the slightly uneven elevator floor often causes one portion of the instrument to reach the optical bench first. Compression in this region will allow the instrument to become parallel with the AO bench as the instrument is raised up. 2) Our cart has fine "x-y" adjustment to match our mounting pucks with the AO bench pucks. The instrument can be rotated on this cart in a "spit" manner--essential for switching between the "optics down" configuration for mounting, and the "optics up" configuration for instrument maintenance.

REFERENCES

[1] Oppenheimer, B. R., "Imaging Exoplanets: The Role of Small Telescopes," The Future of Small Telescopes in The new Millenium. Volume III—Science in the Shadow of Giants, 3, 155 (2003).

[2] Hinkley, S. et al., "Temporal Evolution of Coronagraphic Dynamic Range and Constraints on Companions to Vega," Astrophysical Journal, 654, 633-640 (2007).

[3] Lyot, B., "The study of the solar corona and prominences without eclipses," MNRAS, 99, 580 (1939).

[4] Sivaramakrishnan, A., "Ground-based Coronagraphy with High-order Adaptive Optics," Astrophysical Journal, 552, 397-408 (2001).

[5] Oppenheimer, B. R., "The Lyot Project: Toward Exoplanet Imaging and Spectroscopy," Proc. SPIE 5490, 433 (2004).

[6] Sivaramakrishnan, A., "The Lyot Project: status and results," Comptes Rendus Physique, 8, 355-364 (2007).

[7] Soummer, R. et al., "Stellar Coronagraphy with Prolate Apodized Circular Apertures," Astronomy & Astrophysics, 397, 1161-1172 (2003).

[8] Soummer, R. et al., "Apodized Pupil Lyot Coronagraphs for Arbitrary Telescope Apertures," Astrophysical Journal, 618, L161 (2005).

[9] Racine, R. et al., "Speckle Noise and the Detection of Faint Companions," PASP, 111, 587 (1999)

[10] Soummer et al., "Speckle Noise and Dynamic Range in Coronagraphic Images," Astrophysical Journal, 669, 642 (2007).

[11] Leconte, J. et al., "The Lyot Project: Survey Analysis," Bernard Lyot Conference: The Direct Detection of Planets and Circumstellar Disks in the 21st Century (2007)

[12] Marois, C. et al., "Angular Differential Imaging: A Powerful High-Contrast Imaging Technique," Astrophysical Journal, 641, 556 (2006).

[13] Kuhn, J. et al., "Imaging Polarimetric Observations of a New Circumstellar Disk System", Astrophysical Journal, 553, L189 (2001).

[14] Perrin, M. et al., "Laser Guide Star Adaptive Optics Imaging Polarimetry of Herbig Ae/Be Stars", Science, 303, 5662, pp. 1345 (2004)

[15] Oppenheimer et al., "The Solar-System-Scale Disk Around AB Aurigae," arXiv:0803.3629 (2008)

[16] Sparks, W. B, and H.C Ford, "Imaging Spectroscopy for Extrasolar Planet Detection," Astrophysical Journal, 578, 543 (2002)

[17] Beard, S. et al., "Ultracam camera control and data acquisition system," Proc. SPIE 4848, 218 (2002)

[18] Hayward, T. et al., "PHARO: A Near-Infrared Camera for the Palomar Adaptive Optics System," PASP, 113, 105-118 (2001)

[19] Wynne, C. G., "Correction of atmospheric dispersion in the infrared", MNRAS, 282, 863 (1996)

[20] Dekany, R. et al., "First tip-tilt correction with the Palomar 200-in adaptive optics system," Proc. SPIE 3353, 56 (1998)